Environmental Pollution 266 (2020) 115166

Contents lists available at ScienceDirect

Environmental Pollution

journal homepage: www.elsevier.com/locate/envpol

Determining rainwater chemistry to reveal alkaline rain trend in Southwest China: Evidence from a frequent-rainy karst area with extensive agricultural production☆

Jie Zeng [a], Fu-Jun Yue [b, c, d, *], Si-Liang Li [b, c, d], Zhong-Jun Wang [d], Qixin Wu [e], Cai-Qing Qin [b], Ze-Long Yan [b]

[a] Institute of Earth Sciences, China University of Geosciences (Beijing), Beijing, 100083, China
[b] Institute of Surface-Earth System Science, School of Earth System Science, Tianjin University, Tianjin, 300072, China
[c] Tianjin Key Laboratory of Earth Critical Zone Science and Sustainable Development in Bohai Rim, Tianjin University, Tianjin, 300072, China
[d] Puding Karst Ecosystem Research Station, Institute of Geochemistry, Chinese Academy of Sciences, Anshun, 562100, China
[e] Key Laboratory of Karst Environment and Geohazard, Ministry of Land and Resources, Guizhou University, Guiyang, 550025, China

ARTICLE INFO

Article history:
Received 6 March 2020
Received in revised form
1 July 2020
Accepted 1 July 2020
Available online 9 July 2020

Keywords:
Atmospheric acid substances
Rainwater
Acid neutralization
Ion sources
Karst agricultural production

ABSTRACT

Rainwater chemistry plays an important role in the earth-surficial ecosystem, but studies on rainwater chemical composition of karst agro-ecosystem are rare. To explore the rainwater alkalization and the provenance of components responsible for neutralization, two-years chemical monitoring of rainwater was carried out in a karst agricultural catchment in Southwest China. The main findings suggest that SO_4^{2-}, NO_3^-, Ca^{2+}, and NH_4^+ are the principal ions. All the ionic contents show distinctly seasonal variation (highest in winter) in response to variations in seasonal precipitation because the rain-scour process can efficiently remove atmospheric materials. Source identification indicates that Cl^- and Na^+ are mainly derived from marine input whereas SO_4^{2-} and NO_3^- are controlled by anthropogenic emission, in particular, fixed emission sources. The source of NH_4^+ is attributed to intense agricultural production, while Ca^{2+} and Mg^{2+} are mainly derived from calcite dissolution. The rainwater alkalization caused by the seasonal acid neutralization (via basic components, Ca^{2+} and NH_4^+) is beneficial to crop growth but also reflect agricultural overfertilization. Sulfur controlled the total wet acid deposition (68%–94%) and could be a potential agent of weathering.

1. Introduction

Rainfall is a primary sink of soluble gases (mainly acid materials) and particulate matter in the atmospheric environment (Baker and Scheff, 2007; Szép et al., 2018; Keresztesi et al., 2019; Wei et al., 2019a; Wei et al., 2019b). Both the in-cloud and below-cloud processes can significantly remove atmospheric pollutants and further change the pH and chemical components of rainwater (Larssen et al., 2006; Zhou et al., 2019). Therefore, rainwater chemistry could offer helpful information on air quality and could be applied to identify the sources of atmospheric pollutants, which have undergone numerous physical-chemical processes before being trapped by rainwater (Leong et al., 2017; Keresztesi et al., 2020b). Generally, rainwater major ion chemistry is an indicator of anthropogenic origin, terrestrial source, and sea-salt source (Han et al., 2010; Xu et al., 2015). In addition, the chemical components of rainwater are also affected by several factors, such as meteorology, geography, and environmental protection policies (Szép et al., 2018).

A time-series (2000–2017) study across Europe has shown that the relatively homogenous nature of rainwater chemistry reflects common anti-pollution measures and unitary economic development in Europe (Keresztesi et al., 2019). However, China is a rapidly developing country with uneven economic development between different regions (Wang et al., 2017). Variations in the intensity of human activities (or economic development) have resulted in the emission of different atmospheric pollutants (Mullaugh et al., 2015; Cable and Deng, 2018; Keresztesi et al., 2019), leading to variable rainwater chemistry across China. This phenomenon is particularly

☆ This paper has been recommended for acceptance by Jörg Rinklebe.

* Corresponding author. Institute of Surface-Earth System Science, School of Earth System Science, Tianjin University, Tianjin, 300072, China.
E-mail address: fujun_yue@tju.edu.cn (F.-J. Yue).

https://doi.org/10.1016/j.envpol.2020.115166
0269-7491/

pronounced in less developed areas of Southwest China (globally one of the largest areas of karst geology) (Wang et al., 2017), and includes cities, rural areas and forest areas in Guizhou Province (Han et al., 2019; Zeng et al., 2020a). High levels of precipitation facilitate the migration of materials from the surface to the underground systems and their turnover. The subsequent runoff leads to intense soil erosion in areas with severe karstification (e.g., karst sinkholes, depression, cone, and cockpit) (Zeng et al., 2019a; Zeng and Han, 2020). Moreover, because the capacity for water and nutrient retention in karst agricultural ecosystems is weak, rainfall is the key source of nutrients, solutes and moisture in this region (Hao et al., 2017; Qin et al., 2020).

Previous studies regarding rainwater chemistry in karst areas of Southwest China focused mainly on urban areas (Han et al., 2019). Studies on seasonal variation in rainwater chemistry driven by agriculture (and related essential human activities, e.g., coal-fired heating) in karst areas and their environmental implications, are rarely reported. Given the fragility of the karst agroecosystem, it is essential to improve the understanding of the chemical components of rainwater to facilitate better environmental management and enhanced understanding of the geo-chemical cycle in karst agricultural ecosystems. Moreover, although China underwent periods of severe acid-rain (Larssen et al., 2006), with the implementation of a series of positive measures by the Chinese government, a trend of increasing rainwater alkalinity has been observed across China, particularly in northern China (Yang et al., 2012; Rao et al., 2017), and a similar observation was also found in a typical city in karst region (Guiyang, SW China) in recent years (Han et al., 2019). However, an alkalization trend in vast agricultural areas on karst land has not been confirmed and so there has been no comparison of the drivers of alkalization in different regions.

To advance further information on rainwater chemistry and the rain-scour behavior on atmospheric acid substances and the acid neutralization in a high precipitation karst agro-catchment, two-year samples were obtained, and the time series variations of chemical compositions, electrical conductivity (EC), and pH were systematically studied. The key objectives are to: (1) clarify the link between rain-scour and air acid materials, (2) assess the degree of acid neutralization and its seasonal variation, (3) identify the sources of substances involved in neutralization, and (4) explore the potential environmental implications of rain alkalization on karst ecological restoration.

2. Materials and methods

2.1. Study region

The Houzhai River basin (73.4 km^2), located in the central karst area of Guizhou Province, SW China, was selected as the study region. The elevation of this basin ranges from 1212 to 1552 m (Fig. 1a). The basin is characterized by a subtropical, monsoonal climate (yearly average air temperature 15.1 °C). Most of the rainfall events (~80%) occur in May to October and result in an annual precipitation range of 1200–1400 mm (Li et al., 2010).

The Houzhai River catchment displays widespread development of karst geomorphology (e.g., cone and cockpit). The geology comprises Permian and Triassic limestone and dolomite (Chen et al., 2008; Li et al., 2010). The land cover of the catchment mainly includes agricultural land (dry land and paddy fields), buildings and forest and shrubs (Yue et al., 2015). As shown in Fig. 1b, farmland is primarily dispersed in the middle-lower stream, which accounts for ~41% of the entire catchment, and about two thirds of the farmland are devoted to rice, the remaining third is dry land used for growing corn, while rape and selected vegetables are grown in winter. For agricultural production, di-ammonium phosphate (20–30%), organic fertilizers (20–30%), and urea (40–60%) are widely used three times annually between April and July. Based on the perspective of basin hydrology, one sampling site (HZV, 105°41′15″E, 26°16′09″N, 1220 m asl.) was selected to collect rainwater samples (Fig. 1a). This site is located in the flat plains downstream of the catchment within a mixed usage profile of buildings (Houzhai village) and agricultural land (paddy field and dry land), which represents a heavier anthropogenic influence (Zeng et al., 2020b).

2.2. Sampling and chemical analysis

Rainwater sample collection was performed using a 65 cm diameter polyethylene (PE) sampler installed on a building roof top approximately 8 m above the ground. The PE lid was used to bypass dust fallout on dry days. After each sampling, the samplers were cleaned with deionized-water, air-dried, and lidded and then prepared for the next sampling. The rainwater samples were manually collected daily on rainy days (if the rainfall duration was >1d, one sample was collected per 24 h). Ultimately, 182 rainwater samples were obtained from June 2016 to June 2018. About 76% of the samples were obtained during the rainy season.

A multi-parameter meter (WTW, Multi Line 3320) was used for the determination of electrical conductivity (EC) and pH. The pretreatment of filtration of samples was achieved by acetate membrane filters (Millipore, 0.45 μm). After that, the samples were stored immediately (kept refrigerated at 4 °C in a clean PE bottle) for determination of rainwater chemistry. The continuous-flow analyzer (Skalar, SAN^{++}) with a spectroscopic detector (spectrophotometry) was used to detect the NH_4^+ and NO_3^- concentrations of samples based the Sodium hypobromate oxidation for NH_4^+ and cadmium column reduction for NO_3^-. The concentration of other ions including K^+, Na^+, Ca^{2+}, Mg^{2+}, Cl^-, F^-, and SO_4^{2-} were analyzed by ion chromatography (Thermo Fisher, ICS-Aquion 1100). The details of quality assurance and quality control can be found in the supplementary information (Text S1).

2.3. Calculation methodology

The volume-weighted mean (VWM) concentrations are calculated using the following formula (Li et al., 2019):

$$C = \frac{\sum C_i P_i}{\sum P_i} \quad (1)$$

where C is the VWM ionic concentration, C_i is the ionic concentration of each sample, and P_i is the corresponding precipitation amount. The data on the precipitation amount for the studied period is taken from previous studies with the same study period (Yue et al., 2019), and was monitored at a meteorological station located in the southern catchment. Given the catchment size and the rainfall meteorological drivers, we assume that the variation in precipitation between the sampling site and the meteorological station were negligible.

To characterise fully the rainwater chemical constituents, total cations ($TZ^+ = Na^+ + K^+ + Mg^{2+} + Ca^{2+} + NH_4^+$, in μeq/L), total anions ($TZ^- = SO_4^{2-} + NO_3^- + Cl^- + F^-$, in μeq/L), and their ratios (TZ^+/TZ^-) were applied (Han et al., 2019).

The fractional acidity (FA) caused by the major acid substances (SO_x and NO_x scoured by rainwater) is calculated to explore the of rainwater neutralization by alkaline components, as follows (Balasubramanian et al., 2001):

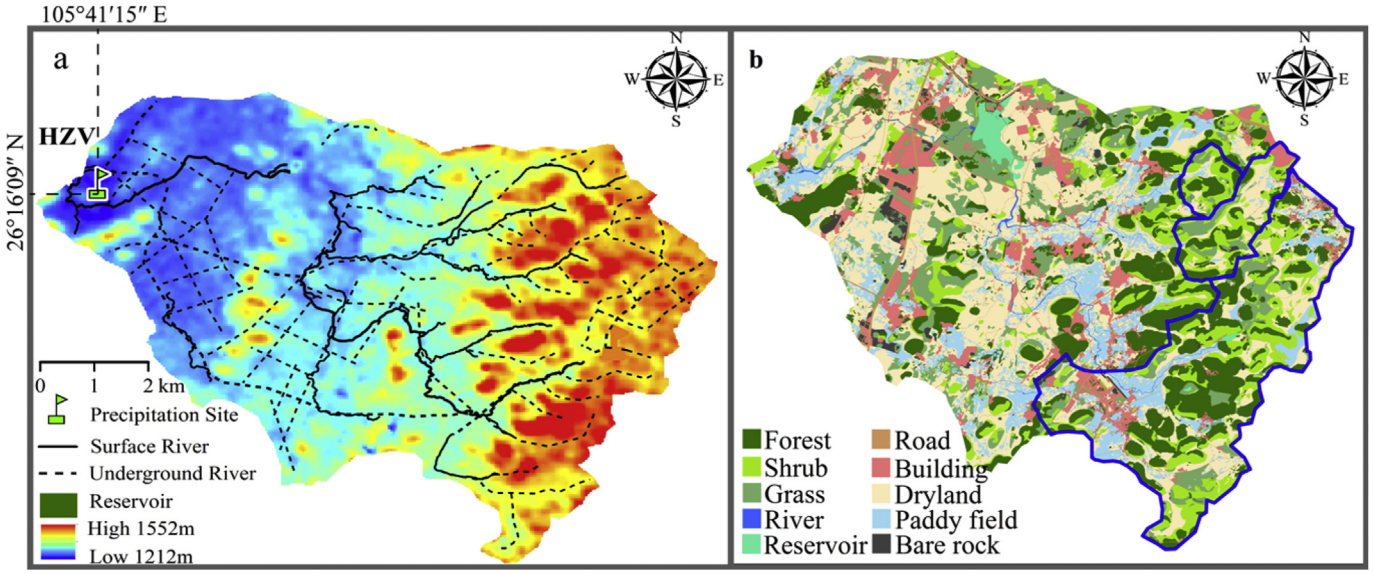

Fig. 1. Map showing the (a) topography and river system, and sampling site; (b) land cover of Houzhai Catchment. Based on a DEM, the flow direction tool in ARCGIS was used to create a direction raster that identifies the drainage area in the study area, land cover was updated based on digitisation from Google Maps, 2016, accessed through QGIS v.2.14.10 open layers plugin, and field validated in May–June 2017 (Buckerfield et al., 2019; Yue et al., 2019; Zhang et al., 2020).

$$FA = \frac{[H^+]}{\left[SO_4^{2-}\right] + NO_3^-} \quad (2)$$

where the $[H^+]$, $[SO_4^{2-}]$, and $[NO_3^-]$ represent the non-sea salt concentrations of these ions (in μeq/L), the pH value is converted to H^+ concentration. If FA = 1, the rainwater acidity has barely been neutralized (Wu et al., 2012).

To obtain further information about the rainwater neutralization by different alkaline components, the neutralization factors (NF) are calculated as follows (Jain et al., 2019):

$$NF_{Xi} = \frac{[X_i]}{\left[SO_4^{2-}\right] + NO_3^-} \quad (3)$$

where $[X_i]$ represent the non-sea salt concentrations of Ca^{2+}, NH_4^+, Na^+, K^+, Mg^{2+} (in μeq/L).

The ratios of neutralizing potential (NP) to acidifying potential (AP) are also calculated as follows (Wu and Han, 2015):

$$NP/AP = \frac{\left[Ca^{2+}\right] + \left[NH_4^+\right]}{\left[SO_4^{2-}\right] + NO_3^-} \quad (4)$$

where $[NO_3^-]$, $[SO_4^{2-}]$, $[NH_4^+]$, and $[Ca^{2+}]$ are the concentrations of the corresponding ion (in μeq/L).

To explore the relationship of rainwater chemistry and typical atmospheric pollutants (SO_2 and NO_2), the monthly atmospheric SO_2 and NO_2 contents are applied. The data source is historical data of air quality in Anshun City, where Houzhai Catchment is located (https://www.aqistudy.cn/historydata/).

2.4. Backward trajectory and positive matrix factorization (PMF)

To explore the potential influence of air mass transport on rainwater chemistry, two days (48h) back trajectories of each rainfall event are computed using the web HYSPLIT model (https://ready.arl.noaa.gov/HYSPLIT_traj.php). All the trajectories are started from 1500m above ground level (AGL) over the sampling site.

The positive matrix factorization (PMF) model is one of the effective methods to evaluate the potential sources of rainwater chemical components (Zhou et al., 2019). This model requires only concentration of each species and the related sample species uncertainty values. The EPA PMF version 5.0 (US) was used in this study.

3. Results and discussion

3.1. Rainwater chemistry and rain-scour effect

3.1.1. Overview of rainwater chemistry

The detailed rainfall, pH, EC, and major ion concentrations of all samples are given in Table S1, and the statistical results (including VWM values) of these parameters are summarized in Table S2. The EC values vary between 3.4 and 204 μS/cm (VWM value = 30.5 μS/cm). Most rainwater samples with high EC values occurred in winter and spring, which is likely controlled by the low rainfall (Table S1). The TZ^+ is slightly higher than TZ^- (Text S1, off the 1:1 line), suggesting that roughly all ionic species were detected (Han et al., 2019). The absence of partial anions could be interpreted as organic anionic species (e.g. plant-released oxalate), which contribute up to 12.6% to the anion (Mullaugh et al., 2014), while the contribution of HCO_3^- is very limited due to the low HCO_3^- content at these pH values (pH < 6.8, VWM value 5.7, Table S2).

There are great variations in ionic content for different precipitation events (Table S2), and the VWM values are therefore suitable for comparison. The VWM concentrations of major ions followed the sequence $Ca^{2+} > NH_4^+ > Na^+ > Mg^{2+} > K^+$ and $SO_4^{2-} > NO_3^- > Cl^- > F^-$ (Table S2).

The proportions of each ion are plotted in Fig. S1, which shows that the principal ions of the rainwater samples are SO_4^{2-}, NO_3^-, Ca^{2+}, and NH_4^+. SO_4^{2-} is the most abundant anion (76.9% of total detected anions), while NO_3^- is the second richest anion with an anion contribution of 17.5% (Fig. S1a). In a cationic pie chart (Fig. S1b), Ca^{2+} is the richest cation and NH_4^+ is the second highest. Although Ca^{2+} (51.7%) play a leading role, NH_4^+ (30.5%) is also an

important contributor of rainwater cations. This can be explained by two factors. First, the widespread carbonate rocks in the karst region provide a plentiful Ca-enriched dust, which further becomes a potential source of Ca^{2+} in rainwater (Han et al., 2019). Second, the application of fertilizer in extensive agricultural production in Houzhai River catchment is also an important source of rainwater Ca^{2+}. This is strongly supported by a previous study on Ca isotopes in rainwater from forested karst areas significantly affected by agriculture (moderate $\delta^{44/40}Ca$ ~ 0.8‰, high NH_4^+/Ca^{2+} and NO_3^-/Ca^{2+} ratios) (Zeng et al., 2020a). Ca^{2+} together with NH_4^+ whose concentration made up 82.2% of the total cations, while SO_4^{2-} and NO_3^- make up 94.4% of the total anions. Therefore, the next sections will focus mainly on these four ions (SO_4^{2-}, NO_3^-, Ca^{2+}, and NH_4^+).

The VWM concentration of rainwater chemicals in the Houzhai catchment, together with those reported data from other karst areas, megacities, deserts, mountainous areas, and oceanic islands, are summarized in Table S3. In this study (karst agricultural catchment), the rainwater NO_3^- concentration was comparative to that in karst city areas but much higher than that in karst virgin forest areas, and the concentration of SO_4^{2-} and Ca^{2+} fall somewhere in between, while the concentration of NH_4^+ was twice that of the former two areas (Han et al., 2010; Han et al., 2019). This reflects the influence of the relative strength of local anthropogenic activities, particularly agriculture, on the chemistry of rainwater in different karst areas. Also, the concentration of most of the ions in Houzhai catchment were significantly lower than that of corresponding ions in inland megacity (Xu et al., 2015) and desert areas (Rao et al., 2017), but higher than that of the corresponding ions of a coastal megacity with huge rainfall amounts (Zhou et al., 2019).

3.1.2. Seasonal variation of rainwater chemistry

Fig. 2 demonstrates that the highest ion concentrations occurred in winter, while the lowest concentrations occurred in summer. All the ion concentrations were slightly higher in spring and fall than in summer. These ion concentration variations were obviously responsive to rainfall amount variations with a significant negative correlation (e.g., Ca^{2+} and rainfall amount, $R = -0.60$, $p < 0.05$; SO_4^{2-} and rainfall amount, $R = -0.58$, $p < 0.05$; Fig. S2). For instance, the monthly behavior of the concentration of dominant cation (Ca^{2+}) mentioned above were also higher in winter (low rainfall amount) but lower in summer (high rainfall amount) (Fig. 2a), which is mainly caused by the fact that more atmospheric dust particles (high Ca^{2+} content) are trapped by raindrops in the rainless winter (Szép et al., 2019), while in the summer season, particularly in June, the rainfall amounts are 387.5 (June 2016) and 345.7 (June 2017) mm, which accounts for almost 30% of the annual precipitation. The frequent rainfall in the summer season has a strong rain-scour effect on atmospheric components, and makes for a shorter atmospheric retention time of pollutants relative to winter (Xiao and Liu, 2002). During the two complete summer periods, the total ion equivalent concentration of rainwater was only one-sixth to one-quarter of that of winter (Fig. 2). Interestingly, under the conditions of almost equal amounts of precipitation, NH_4^+ concentration exhibited an obvious upward trend in early spring (March 2017 and March 2018) compared to the previous winter (Fig. 2a). One possible interpretation of this observation can be that the increasing NH_3 emission from the winter-accumulated ammonium nitrogen in soil, and human and animal excreta (Zhang et al., 2014; Liu et al., 2020) due to the increased air temperature from winter (0.9, 1.1 and 3.5 °C for December, January and February, www.geodata.cn) to early spring (7.8 °C for March).

Similarly, the abundant anions (SO_4^{2-} and NO_3^-) were shown to have the same temporal variation. It is noteworthy that the high concentrations of these anions were accompanied by higher atmospheric SO_2 and NO_2 content (Fig. 2b), with a significant positive correlation between rainwater SO_4^{2-} and atmospheric SO_2 ($R = 0.83$, $p < 0.05$), and between rainwater NO_3^- and atmospheric NO_2 ($R = 0.58$, $p < 0.05$; Fig. S2). Therefore, the high concentrations of rainwater SO_4^{2-} and NO_3^- in winter were not only related to the low precipitation amount and rainfall frequency (Wu et al., 2012; Jain et al., 2019), but also significantly influenced by the content of atmospheric acid substances (SO_2 and NO_2). Increased sulfur oxides and nitrogen oxides will accumulate in the atmosphere with the increased coal combustion requirements in winter (e.g., heating requirements of dwellings, and coal-fired power plants) (Jia and Chen, 2010; Zeng et al., 2020b), which will also subsequently result in high levels of water-soluble sulfates and nitrates in atmospheric particulates through a series of photochemical reactions (Baker and Scheff, 2007; Wei et al., 2020). Moreover, the sulfates and nitrates in rain-scoured atmospheric particulate matter also contribute some SO_4^{2-} and NO_3^- to rainwater in winter (Xiao and Liu, 2004; Elliott et al., 2015).

3.1.3. Rain-scour effect

To explore further the rain-scour effect, the monthly accumulated rainfall amount and abundant ions (including SO_4^{2-}, NO_3^-, Ca^{2+}, NH_4^+, and Mg^{2+}) concentration were analyzed by fitting (Fig. 3). It is clear that these ions have a negative natural logarithmic relationship with the monthly accumulated rainfall amount. As mentioned above, the VWM concentrations of Ca^{2+}, NH_4^+, Mg^{2+}, SO_4^{2-}, and NO_3^- are lower when the monthly cumulative amount of rainfall is large, while the VWM concentrations are higher when the amount of rainfall is small. These observations indicate that rainwater has a preferential removal efficiency and scouring effect on the acidic and alkaline substances in the atmosphere, such as the gaseous sulfur oxides and nitrogen oxides, particulate nitrate and gaseous HNO_3, aerosol NH_4^+ or gaseous ammonia, and particulate Ca/Mg-mineral. Previous studies have also shown that rainfall is an important removal mechanism of these materials (Silva et al., 2009; Szép et al., 2018). Furthermore, it is noteworthy that the VWM concentrations of these ions varied in a relatively stable range when the accumulated rainfall amount exceeded 50 mm (Fig. 3, grey box), which suggest that the atmospheric substances (e.g., gaseous sulfur and nitrogen oxides, aerosol NH_4^+, and suspended carbonate rock particles) were basically scoured completely at this time, and the ion concentrations of rainwater were close to the ion concentrations of cloud-water (atmospheric clouds), reflecting the within-cloud process (Rao et al., 2017). The concentrations fluctuate greatly when the amount of rainfall is less than 50 mm (Fig. 3), which mainly indicates the rain-scour process of the atmosphere below the cloud (Jia and Chen, 2010).

3.2. Alkalization trend (acid neutralizing capacity)

3.2.1. pH distribution

As summarized in Table S2, the rainwater pH values in the studied area vary from 3.8 to 6.8, with a mean value of 5.6 and a VWM value of 5.7. The distribution of rainwater pH (in percentage) in Houzhai catchment is plotted in Fig. S3. Most rainwater samples (66.1%) presented a pH value greater than 5.6 in the study catchment, and 45.8% of them are greater than 6 (Fig. S3). These pH values are beyond the acidity of natural rainwater (rainwater pH in natural atmosphere should range from 5.0 to 5.6 because of the solvation of airborne nitrogen oxides, sulfur oxides, and carbon dioxide in raindrops/clouds) (Galloway et al., 1993), which denotes large alkaline-components inputs. The relative high rainwater pH observed here can be explained by the solvation of ammonia and atmospheric dust, deriving from agriculture (including animal waste, e.g., cattle breeding) and atmospheric particulate matter/resuspended particles (high calcium/magnesium carbonate content)

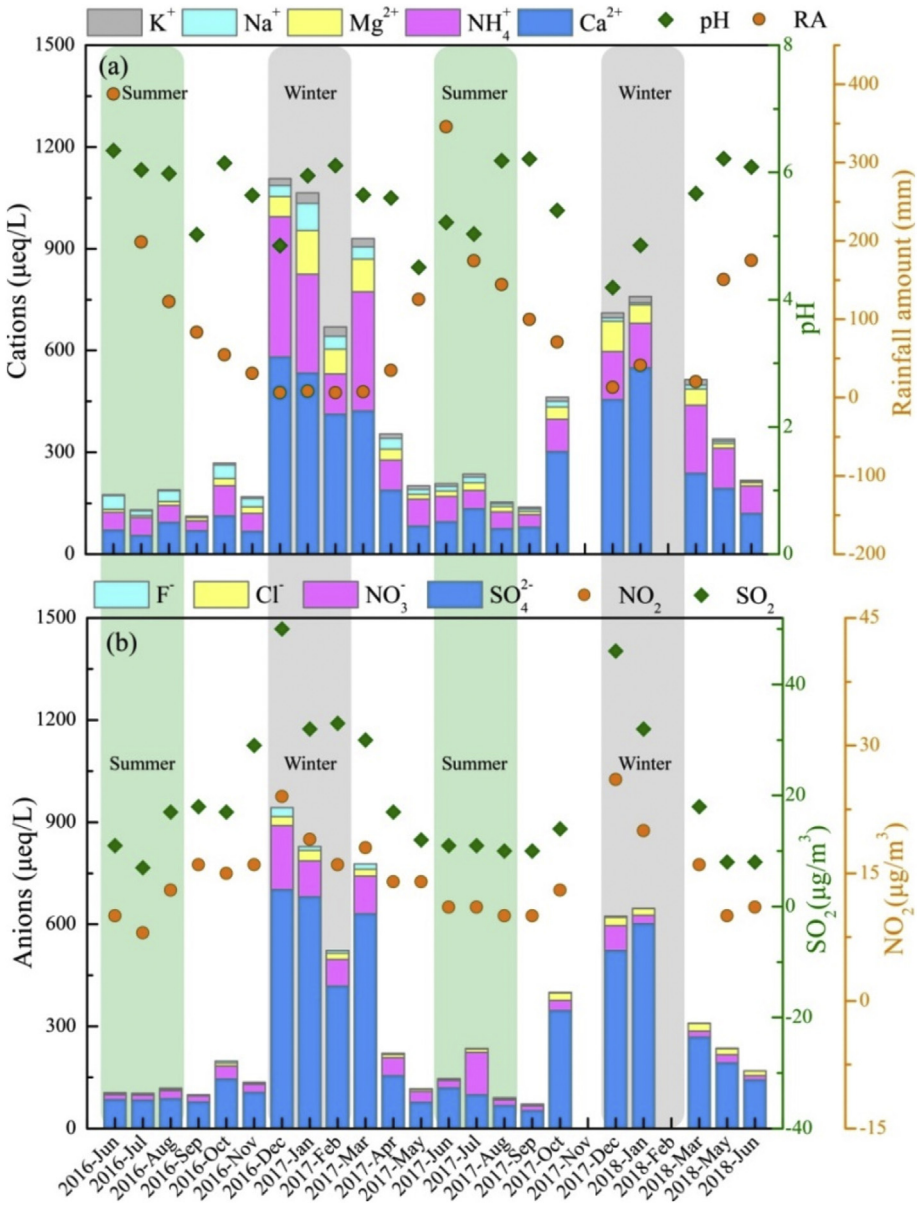

Fig. 2. Monthly variations of cation (a) and anion (b) concentration, pH, rainfall amount (RA), and atmospheric SO_2 and NO $_2$ content. The monthly atmospheric SO_2 and NO_2 are from historical data of air quality in Anshun City, where Houzhai Catchment is located (https://www.aqistudy.cn/historydata/).

within the study region. Nevertheless, the pH of our karst rainwater is far below that of the desert rainwater extremely influenced by dust in northwest China (pH = 7.6, Table S3) (Rao et al., 2017). Moreover, 4% of samples from winter rainwater exhibited an extremely low pH (<4) (Fig. S3 and Table S1), which demonstrates the potential anthropogenic acid input to the ecological system in this season, such as the SO_x and NO_x emission derived from the heating requirements of dwellings (coal combustion) and potential biomass burning.

3.2.2. Seasonal acid neutralization

The rainwater alkalization (large proportion of high pH samples, Fig. S3) and the presence of the main acidifying components (SO_4^{2-} and NO_3^- are dominant anions, Fig. S1a), observed in this study imply an intense acid neutralization during the precipitation process, which can be further supported by the significant correlations between rainwater acidic ions (SO_4^{2-} and NO_3^-, $p < 0.05$), atmospheric acid gas (SO_2 and NO_2, $p < 0.05$), and the base cations (Fig. S2). According to the VWM concentrations of relevant ions involved in Equation (2) (Balasubramanian et al., 2001), the FA value of the rainwater during the whole study period is calculated as 0.0122, suggesting that roughly 98.78% of precipitation acidity is neutralized by basic substances. This neutralizing capacity is much stronger than the average European levels (FA = 0.3, 70% of rainwater acidity is neutralized in many developed countries) (Keresztesi et al., 2019).

The acidity produced by sulfuric and nitric acids are trapped and neutralized by gaseous alkali and base cations (Wu and Han, 2015). According to Equation (3), the rainwater acid neutralization by these alkaline components is confirmed by evaluating the NF. The calculation results of the whole period under study, show that the NF values of Ca^{2+}, NH_4^+, Na^+, Mg^{2+}, and K^+ of rainwater are 0.75, 0.45, 0.12, 0.08, and 0.04, respectively. This reveals that Ca^{2+} and NH_4^+ are the principal contributors to rainwater acid neutralization,

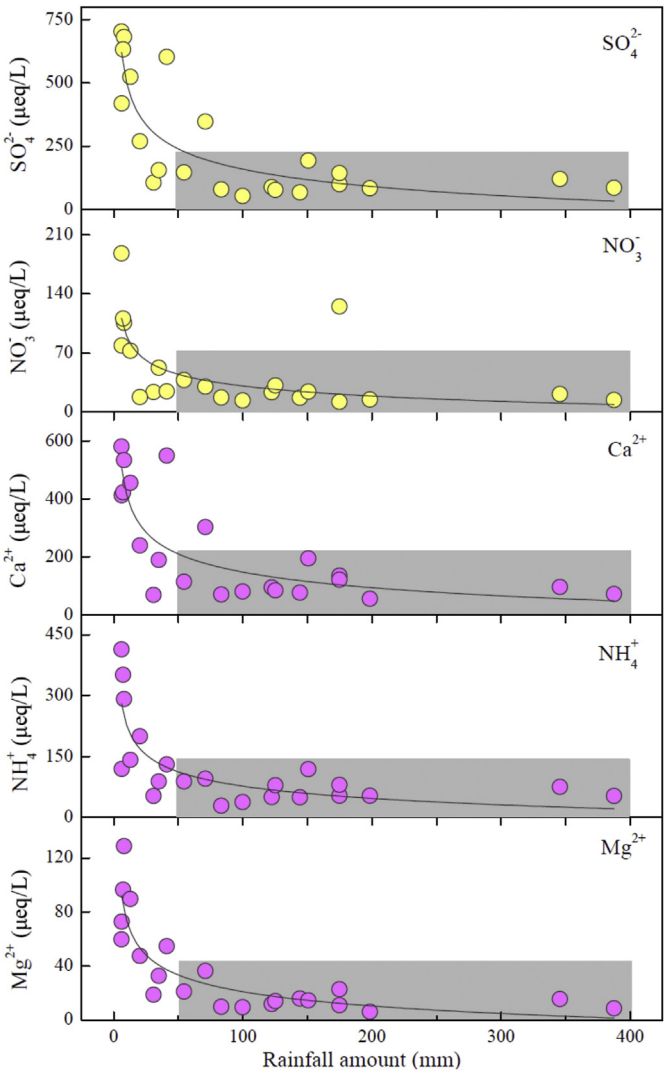

Fig. 3. The relationship of Monthly VWM ion concentration and the monthly cumulative rainfall reflect the rain-scour effect on atmospheric substances.

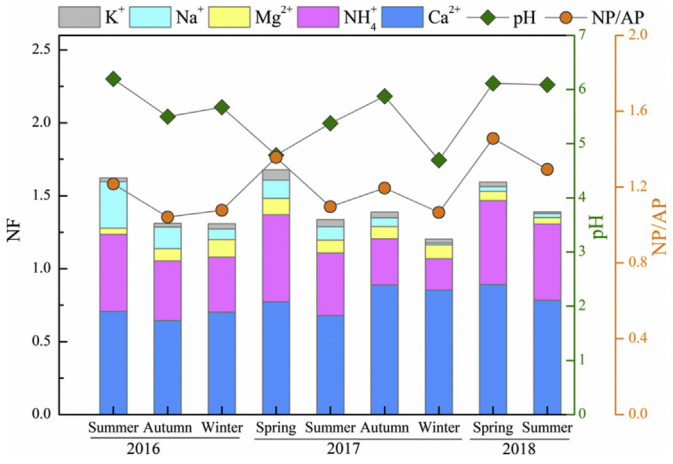

Fig. 4. Seasonal variations of neutralization factors (NF) and the ratio of neutralizing potential to acidifying potential (NP/AP) at Houzhai catchment.

which is in line with the finding of a previous study at the adjacent site (Lü et al., 2017). Compared to the developed areas where Na^+ has the strongest neutralizing capacity (mean NF = 0.54, ranging from 0.04 to 0.98), followed by NH_4^+ (mean NF = 0.46, ranging from 0.03 to 1.25) (Keresztesi et al., 2019), our results indicate that the widespread existence of potential calcium and ammonia sources in karst agricultural areas provides powerful support for the alkalization trend of Na-depleted rainwater.

To understand further the seasonal variations of acid neutralization, the seasonal VWM values relevant in Equation (3) are also calculated and plotted in Fig. 4. Overall, a higher NF value is observed in spring and summer, indicating that the rainfall was more neutralized during these seasons, which is strongly influenced by the seasonal variations of the neutralization-involved ions mentioned before. Significantly, the NF of Ca^{2+} accounts for a predominant percentage during the whole period under study, with a minor seasonal variation, which is controlled by the high Ca background value in karst regions. While the NF values of NH_4^+ vary in seasonally (higher in spring and summer but lower in fall and winter), this is related to the enhanced agricultural production and more efficient ammonia emissions in spring and summer (Wang et al., 2020). The relatively low proportion of NFs of Mg^{2+}, Na^+, and K^+ in each season reveals that the neutralization by these ions is negligible (Fig. 4).

The ratios of rainwater neutralizing potential (NP) to acidifying potential (AP) are also calculated to evaluate the acidity and alkalinity balance (Wu and Han, 2015). It can be seen from Fig. 4 that the variations of NP/AP ratio are almost always accompanied by similar variations of pH (except for Spring 2017), implying that alkaline components neutralize rainwater acidity and therefore affect the pH in different seasons. Our NP/AP ratio is significantly higher than in Europe (NP/AP = 0.46–0.80) where rainwater is predominantly acidic in character (Keresztesi et al., 2019). This also further explains the pH distribution of karst agricultural rainwater (66.1% of samples present a non-acidic character, Fig. S3).

3.3. Source of the major ions

3.3.1. Source identification

Based on the similar chemical characteristics and the possible co-emission origins of some atmospheric components (e.g., SO_2 and NO_x) (Vet et al., 2014), the correlation analysis is therefore a common method to distinguish the potential common origins of rainwater ionic components, which are calculated and shown in Fig. S2. As seen in Fig. S2, the rainwater pH does not exhibit significant correlations with all ions ($p > 0.05$) but does show a significant negative correlation with atmospheric SO_2 and NO_2 ($p < 0.05$), which confirms the seasonal acid neutralization mentioned above. However, significant positive correlations are observed among almost all the ions ($p < 0.05$, Fig. S2). Therefore, it is difficult to obtain more information about ion sources via correlation analysis.

The rainwater samples in our study catchment are plotted on the SO_4^{2-} and NO_3^- line and tend to the SO_4^{2-} end in the ternary diagrams (Fig. S4 a), and almost all samples present a SO_4^{2-}/NO_3^- ratio >1 (Table S1). Compared to the marine area (the samples tend to the Cl^- end; Fig. S4a), our results reflect that the anion compositions of rainwater are predominantly controlled by anthropogenic emissions (Han et al., 2010), particularly affected by the fixed emission sources (based on the high SO_4^{2-}/NO_3^- ratio), such as transmission of regional emissions from coal combustion (Arimoto et al., 1996; Walters et al., 2015; Li et al., 2020). In the ternary diagram of cations, most of the rainwater samples in this study are plot on the line between the ends of NH_4^+ and $[Ca^{2+} + Mg^{2+}]$ (Fig. S4 b), indicating the cations are primarily influenced by mixed sources of continental input and human activity (Zeng et al., 2019b;

Keresztesi et al., 2020a), while the contribution of marine input to the rainwater cations is relatively low, which can be supported by the cation compositions of the oceanic island (Fig. S4b).

To identify further the relationships between ionic species and their sources, the variations of SO_4^{2-}/Na^+, NO_3^-/Na^+, NH_4^+/Na^+ with Cl^-/Na^+ and Mg^{2+}/Ca^{2+} with SO_4^{2-}/Ca^{2+} ratios in rainwater are plotted in Fig. 5. It can be seen from Fig. 5a that approximately a quarter of the rainwater samples have high Cl^-/Na^+ ratios (relative to seawater), while the Cl^-/Na^+ ratios of most of the samples are less than that of seawater (Berner and Berner, 1987). This indicates that the human-derived Cl^- is relatively limited, and that mineral-weathered Na^+ (e.g., potential silicate hydrolysis when the atmospheric cloud crossed the silicate regions of south China) may additionally be input to the air, causing a lower Cl^-/Na^+ ratio in most cases (Rao et al., 2017). Moreover, the high SO_4^{2-}/Na^+ and NO_3^-/Na^+ ratios of most rainwater samples (Fig. 5a and b) further support the control of the rainwater SO_4^{2-} and NO_3^- from the anthropogenic emissions mentioned above (Fig. S4). The mobile sources that contributed rainwater NO_3^- can be muted due to the dilution effect present during long-distance transport/diffusion (Rao et al., 2017; Zeng et al., 2019b). The significantly high NH_4^+/Na^+ ratio (~56) compared to the Cl^-/Na^+ ratio (all the Cl^-/Na^+ ratios < 4.8) were also shown in Fig. 5c. Therefore, although the positive correlation between Cl^- and NH_4^+ ($R = 0.78$, $p < 0.05$) is observed in Fig. S2, these two ions have different origins to some degree. According to previous studies, the gaseous NH_3 produced by agriculture-associated fertilizer, animal waste, and biomass burning can be the major sources of NH_4^+ in rainwater (Lee et al., 2012; Rao et al., 2017), which is further supported by the high NH_4^+/NO_3^- ratios of the rainwater (up to 37.5 with a mean value of 4.3), suggesting that agriculture is the primary origin of NH_4^+ in rainwater in the studied catchment (Lee et al., 2012; Zeng et al., 2020b). Moreover, the seasonal farming practices including fertilizer application and biomass burning can be one of the interpretations for seasonal variations of rainwater NH_4^+. In Fig. 5d, all the rainwater samples are distributed among the [calcite + dolomite] dissolution line and calcite dissolution line with low Mg^{2+}/Ca^{2+} ratio (<0.5), indicating that the rainwater Ca^{2+} and Mg^{2+} are mainly controlled by calcite solvation of air dust derived from differential carbonate weathering (Lü et al., 2017).

3.3.2. Backward trajectory analysis

The typical back-trajectories are defined as three sectors and the representative trajectories are shown in Fig. S5. The VWM concentrations of major ions of these three sectors are summarized in Table S4. The variations of concentration of most ions are not obvious between different sectors (Table S4).

The highest NO_3^- concentration is found in sector 2 (North and Northeast, Fig. S5), corresponding to the big cities in this direction (e.g., Chengdu, Chongqing, and Guiyang). These cities are heavily contaminated by their heavy traffic and are the potential sources of NO_x for long-distance transportation, which can be further supported by the highest NO_3^-/SO_4^{2-} ratio of rainwater in this sector (Table S4). The relatively higher NH_4^+ concentration is associated

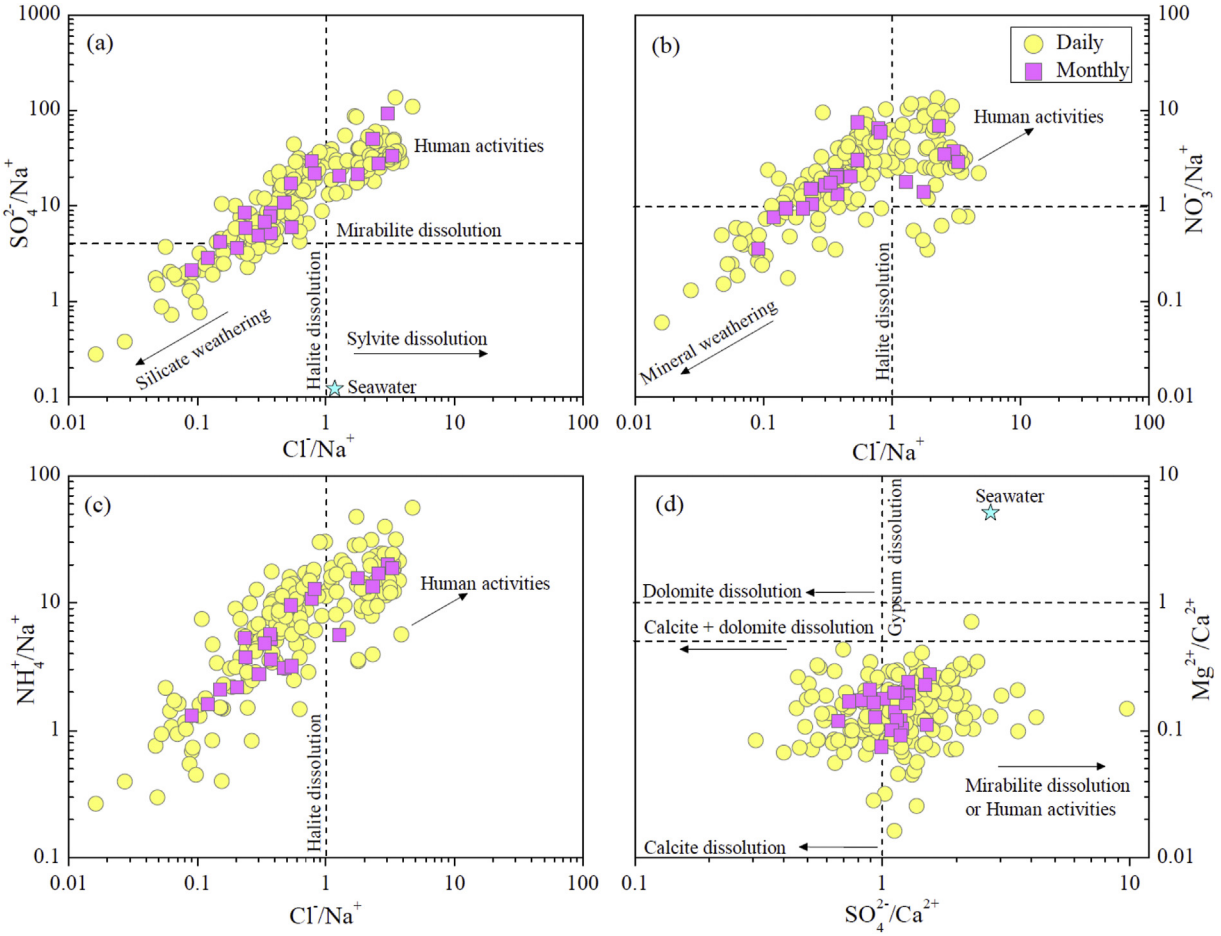

Fig. 5. The daily and monthly variations of SO_4^{2-}/Na^+, NO_3^-/Na^+, NH_4^+/Na^+ with Cl^-/Na^+ and Mg^{2+}/Ca^{2+} with SO_4^{2-}/Ca^{2+} ratios (equivalent ratio) in rainwater at Houzhai catchment. Data sources for seawater and the imaginary line are from (Berner and Berner, 1987).

with associated with sector 1 (West and Southwest, Fig. S5), as this direction is relatively less polluted and more potential agricultural source regions are distributed in border area of Yunnan-Guizhou provinces. In contrast, the highest SO_4^{2-} concentration is observed in sector 3 (South and Southeast, Fig. S5). Rainwater related trajectory of this direction is characterized by high load of SO_4^{2-} (typical anthropogenic pollutants) but lowest NO_3^-/SO_4^{2-} ratio compared with other sectors. This observation supports the developed industries in this direction, which can be responsible for the potential source of sulfate for long-distance transportation. These findings suggest that the impact of long-distance transportation of pollutants on rainwater chemistry is non-negligible in the study catchment.

3.3.3. Source contributions

Based on the previous discussion, the marine input, crust dust, and anthropogenic emissions are confirmed as the main contributors of rainwater ions. Three factors well fitted to the data based on the physically interpretable source, and the chemical source profiles obtained from PMF model are shown in Fig. S6. As shown in Fig. S6, Factor 1 (F1) explains 80% of the Ca^{2+}, 68% of the Mg^{2+}, 58% of the K^+, 71% of SO_4^{2-}, and 84% of Cl^-. This factor can be interpreted as the contributions from dusts, which may integrate natural dust (high load of representative crust substance Ca^{2+}) and human-influenced dust (inferred from the high load of SO_4^{2-} in F1, e.g., sulfate-adsorbed dust). Factor 2 (F2) with highest contribution of most typical sea salt Na^+ (96%) represents the marine input, which reflected the impact of marine aerosols. Nitrogen species and fluorine were important components in Factor 3 (F3, anthropogenic input), with the highest contribution of NO_3^- (86%), NH_4^+ (76%), and F^- (71%). These species in F3 are typical markers of human-related secondary aerosol particles (e.g., NH_4NO_3) that produced by the NO_x oxidation (Rao et al., 2016).

3.4. Implications on karst biogeochemistry cycle

As early as the end of the twentieth century, the study area has been considered to be an acid rain control area, and the Houzhai catchment is located in the middle of the Chongqing – Guiyang – Liuzhou acid rain region (Larssen et al., 2006). However, although the variations of most of the rainwater ion concentrations do not exhibit a significant trend in the last decade (Fig. 6), the most primary acid ion (SO_4^{2-}) deposition in this karst catchment basically shows a downward trend (Fig. 6b, the significantly low SO_4^{2-} concentration in 2015 wet season was caused by the strong dilution effect during the study period). This can be explained by the effective implementation of a series of environmental protection policies over China, such as the National Acid Rain and SO_2 Pollution Prevention Plan in the past several years (Yu et al., 2019), which effectively reduces the emission of acidic gas pollutants and causes the decreased SO_4^{2-} concentration. In contrast, the NO_3^- concentration shows a slight upward trend (Fig. 6b), which may be related to increasing NO_x emissions from agriculture caused by farmers continuously increasing the application of fertilizer for more crop production (Yue et al., 2015), in particular, under the background of the Chinese Grain for Green Program (Song et al., 2014). Moreover, because of intense and extensive agriculture, a significantly increased concentration of rainwater NH_4^+ was observed from 2008 to 2018 (Fig. 6b), which is an important participant in acid neutralization as has been discussed before. Therefore, both the decrease of acid-producing ionic concentration (e.g., SO_4^{2-}) and the increase of neutralization ionic concentration (e.g., NH_4^+) resulted in the increasing trend of pH value 2008 to 2018, that is, rainwater alkalization. Similar rainwater alkaline trends were also observed in the Alxa Desert and Beijing (Northern China) (Yang et al., 2012; Rao et al., 2017), but the drivers were different. Alkalization of rainwater in north China is caused by the widespread sandstorms that contribute a large amount of Ca and Mg to rainwater and neutralize the acidic ions, whereas the NH_3 emission from agriculture is also a significant driving factor in this study. Overall, the increase concentrations of NO_3^- and NH_4^+ in rainwater would provide N sources to N depletion ecosystem (Gao et al., 2019), e.g. natural forest and shrub. Meanwhile the phenomenon of acid neutralization reduced the hazard of acid rain to crops (particularly foliar level) (Feng et al., 2002; Singh and Agrawal, 2008). All of these benefited to ecological restoration of karst area in southwest China (Wu et al., 2020; Tong et al., 2020). However, increase concentrations of NO_3^- and NH_4^+ in rainwater also reflects the excessive application of fertilizer in agricultural production, resulting in a great waste of resource.

Previous studies have shown that the long-term application of synthetic nitrogenous fertilizer in the study area has caused an increase of ~0.2 t/(km^2·yr) over the past 20 years (Yue et al., 2015), resulting in high levels of nitrogen in aquatic systems and rainwater. Moreover, inorganic nitrogen deposition contributes 68.7% of total nitrogen deposition (Zeng et al., 2020b), and the annual mean atmospheric inorganic nitrogen deposition flux can be calculated as 115.3 mmol N/(m^2·yr) based on the amount of rainfall and inorganic nitrogen concentrations ($NH_4^+ + NO_3^-$) (Table S1). Meanwhile, nitrogen-related deposition and nutrient can change

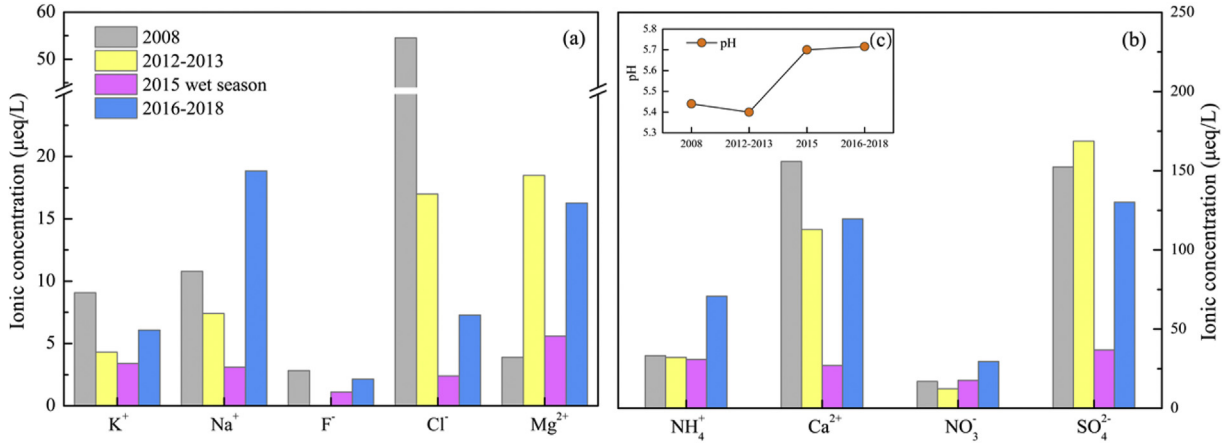

Fig. 6. The variations in ions concentrations (μeq/L) of rainwater in Houzhai River catchment during the last decade, the data for 2008 (Wu et al., 2012), 2012–2013 (Lü et al., 2017), and 2015 wet season (Zeng et al., 2019b) are from the adjacent monitoring sites.

gross primary productivity (GPP) in earth-surface aquatic system (Gao et al., 2019). GPP is the C absorption amount via photosynthesis in ecosystems and a key role in terrene-air CO_2 exchange (Hao et al., 2019). According to the GPP of 1000–1500 g C/(m^2·yr) in the studied areas (Hao et al., 2019) and the Redfield C/N ratio (6.625:1), it can be calculated that the GPP of Houzhai catchment is equivalent to 12,579–18,868 mmol N/(m^2·yr). Therefore, we roughly estimate that the contribution of rainwater inorganic nitrogen deposition (115.3 mmol N/(m^2·yr)) to GPP accounts for 0.61%–0.92%.

In addition, although the rainwater was highly neutralized, the surface water acidification, driven by rainwater-input nitrate and sulfate, combined with protons in the aquatic ecosystems, has been a subject of concern (Pan et al., 2013; Qiao et al., 2018), which could be extensively involved in and significantly affected by the carbonate rocks weathering in karst regions (Li et al., 2008; Yue et al., 2015; Liu and Han, 2020), and further affect global climate change (Raymond et al., 2013; Wang et al., 2019). Our previous studies showed that the enhanced carbonate rock weathering HCO_3^- flux of the surfacewater-groundwater system in Houzhai catchment would be 3.72×10^5 kg C/yr (18.7% of total HCO_3^- flux) as a result of nitrification process (Yue et al., 2015), while up to 42% of the divalent cations originated from the carbonate weathering involved with sulfuric acid (Li et al., 2008). The seasonal wet acid deposition in Houzhai catchment varied from 0.15 to 1.0 keq/ha (Fig. S7), and the annual wet acid deposition is therefore calculated as 1.9 keq/(ha·yr) in 2017. This value is consistent with the observation in the Yangtze River Deltas (mean value of 2.0 keq/(ha·yr) (Chen et al., 2019)). However, our results do not support the previous findings indicating that the nitrate controlled the total wet acid deposition (Pan et al., 2013), which is mainly attributed to the differences in the nitrogen sources. In contrast, the contribution of sulfur to total wet acid deposition (68%–94%) is significantly higher than that of nitrate (Fig. S7). Therefore, the rainwater-related surface water acidification and its environmental effects, particularly sulfate as a potential agent of weathering, need more long-term deposition monitoring in the karst area.

4. Conclusions

In conclusion, two-year rainwater samples were collected in a karst agricultural catchment to investigate the rainwater chemistry and rainwater alkalization. The stoichiometric and time-series rainwater chemistry effectively interprets the alkalify process of rainwater. SO_4^{2-}, NO_3^-, Ca^{2+}, and NH_4^+ are the primary ions in rainwater with distinctly seasonal variation. Rain-scour process can effectively remove atmospheric substances. Source apportionment indicated that SO_4^{2-} and NO_3^- are controlled by anthropogenic emission, while crustal sources (e.g., calcite dissolution of continental dust) are the main sources of K^+, Mg^{2+}, and Ca^{2+}. NH_4^+ is mainly controlled by agriculture. Although rainwater alkalization is beneficial to plant growth, a focus on sulfur-related deposition (potential agent of weathering) is required.

CRediT authorship contribution statement

Jie Zeng: Investigation, Data curation, Formal analysis, Writing - original draft. **Fu-Jun Yue:** Conceptualization, Supervision, Writing - review & editing. **Si-Liang Li:** Conceptualization, Supervision, Writing - review & editing. **Zhong-Jun Wang:** Formal analysis, Methodology, Investigation, Writing - review & editing. **Qixin Wu:** Data curation, Writing - review & editing. **Cai-Qing Qin:** Data curation, Investigation, Writing - review & editing. **Ze-Long Yan:** Data curation, Investigation.

Declaration of competing interest

The authors declare that they have no known competing financial interests or personal relationships that could have appeared to influence the work reported in this paper.

Acknowledgments

The authors thank all anonymous reviewers for their helpful comments and Prof. Robert M. Ellam who come from Scottish Universities Environmental Research Centre, United Kingdom to improve the language. This research was funded by the Strategic Priority Research Program of Chinese Academy of Sciences, Grant No. XDB40020503; National Natural Science Foundation of China [grant numbers 41925002, 41571130072]; and the Independent Innovative Foundation of Tianjin University [grant number 2020XY-0025].

Appendix A. Supplementary data

Supplementary data to this article can be found online at https://doi.org/10.1016/j.envpol.2020.115166.

References

Arimoto, R., Duce, R.A., Savoie, D.L., Prospero, J.M., Talbot, R., Cullen, J.D., Tomza, U., Lewis, N.F., Ray, B.J., 1996. Relationships among aerosol constituents from Asia and the North Pacific during PEM-West A. J. Geophys. Res. Atmos. 101, 2011–2024.

Baker, K., Scheff, P., 2007. Photochemical model performance for PM2.5 sulfate, nitrate, ammonium, and precursor species SO_2, HNO_3, and NH_3 at background monitor locations in the central and eastern United States. Atmos. Environ. 41, 6185–6195.

Balasubramanian, R., Victor, T., Chun, N., 2001. Chemical and statistical analysis of precipitation in Singapore. Water Air Soil Pollut. 130, 451–456.

Berner, E.K., Berner, R.A., 1987. Global Water Cycle: Geochemistry and Environment. Prentice-Hall, New York.

Buckerfield, S.J., Quilliam, R.S., Waldron, S., Naylor, L., Li, S., Oliver, D.M., 2019. Rainfall-driven E. coli transfer to the stream-conduit network observed through increasing spatial scales in mixed land-use paddy farming karst terrain. Water Research X, p. 100038.

Cable, E., Deng, Y., 2018. Trace elements in atmospheric wet precipitation in the detroit metropolitan area: levels and possible sources. Chemosphere 210, 1091–1098.

Chen, X., Chen, C., Hao, Q., Zhang, Z., Shi, P., 2008. Simulation of rainfall-underground outflow responses of a karstic watershed in Southwest China with an artificial neural network. Water Sci. Eng. 1, 1–9.

Chen, Z., Huang, T., Huang, X., Han, X., Yang, H., Cai, Z., Yao, L., Han, X., Zhang, M., Huang, C., 2019. Characteristics, sources and environmental implications of atmospheric wet nitrogen and sulfur deposition in Yangtze River Delta. Atmos. Environ. 219, 116904.

Elliott, E.M., Kendall, C., Boyer, E.W., Burns, D.A., Lear, G.G., Golden, H.E., Harlin, K., Bytnerowicz, A., Butler, T.J., Glatz, R., 2015. Dual nitrate isotopes in dry deposition: utility for partitioning NO_x source contributions to landscape nitrogen deposition. J. Geophys. Res. Biogeosci. 114, 425–453.

Feng, Z.W., Miao, H., Zhang, F.Z., Huang, Y.Z., 2002. Effects of acid deposition on terrestrial ecosystems and their rehabilitation strategies in China. J. Environ. Sci. 14, 227–233.

Galloway, J.N., Savoie, D.L., Keene, W.C., Prospero, J.M., 1993. The temporal and spatial variability of scavenging ratios for NSS sulfate, nitrate, methanesulfonate and sodium in the Atmosphere over the North Atalantic Ocean. Atmos. Environ. Part A. General Topics 27, 235–250.

Gao, Y., Jia, Y., Yu, G., He, N., Zhang, L., Zhu, B., Wang, Y., 2019. Anthropogenic reactive nitrogen deposition and associated nutrient limitation effect on gross primary productivity in inland water of China. J. Clean. Prod. 208, 530–540.

Han, G., Song, Z., Tang, Y., Wu, Q., Wang, Z., 2019. Ca and Sr isotope compositions of rainwater from Guiyang city, Southwest China: implication for the sources of atmospheric aerosols and their seasonal variations. Atmos. Environ. 214, 116854.

Han, G., Tang, Y., Wu, Q., Tan, Q., 2010. Chemical and strontium isotope characterization of rainwater in karst virgin forest, Southwest China. Atmos. Environ. 44, 174–181.

Hao, Z., Gao, Y., Sun, X., Wen, X., Xiong, B., 2019. Determining nitrogen and carbon footprints to reveal regional gross primary productivity and differentiation characteristics in karst and non-karst watersheds, China. J. Clean. Prod. 227, 1149–1160.

Hao, Z., Gao, Y., Yang, T., Tian, J., 2017. Atmospheric wet deposition of nitrogen in a

subtropical watershed in China: characteristics of and impacts on surface water quality. Environ. Sci. Pollut. Control Ser. 24, 8489–8503.
Jain, C.D., Madhavan, B.L., Ratnam, M.V., 2019. Source apportionment of rainwater chemical composition to investigate the transport of lower atmospheric pollutants to the UTLS region. Environ. Pollut. 248, 166–174.
Jia, G., Chen, F., 2010. Monthly variations in nitrogen isotopes of ammonium and nitrate in wet deposition at Guangzhou, south China. Atmos. Environ. 44, 2309–2315.
Keresztesi, Á., Birsan, M.-V., Nita, I.-A., Bodor, Z., Szép, R., 2019. Assessing the neutralisation, wet deposition and source contributions of the precipitation chemistry over Europe during 2000–2017. Environ. Sci. Eur. 31, 50.
Keresztesi, Á., Nita, I.-A., Birsan, M.-V., Bodor, Z., Pernyeszi, T., Micheu, M.M., Szép, R., 2020a. Assessing the variations in the chemical composition of rainwater and air masses using the zonal and meridional index. Atmos. Res. 237, 104846.
Keresztesi, Á., Nita, I.-A., Birsan, M.-V., Bodor, Z., Szép, R., 2020b. The risk of cross-border pollution and the influence of regional climate on the rainwater chemistry in the Southern Carpathians, Romania. Environ. Sci. Pollut. Res. 27, 9382–9402.
Lü, P., Han, G., Wu, Q., 2017. Chemical characteristics of rainwater in karst rural areas, Guizhou Province, Southwest China. Acta Geochimica 36, 572–576.
Larssen, T., Lydersen, E., Tang, D., He, Y., Gao, J., Liu, H., Duan, L., Seip, H.M., Vogt, R.D., Mulder, J., Shao, M., Wang, Y., Shang, H., Zhang, X., Solberg, S., Aas, W., Okland, T., Eilertsen, O., Angell, V., Li, Q., Zhao, D., Xiang, R., Xiao, J., Luo, J., 2006. Acid rain in China. Environ. Sci. Technol. 40, 418–425.
Lee, K.-S., Lee, D.-S., Lim, S.-S., Kwak, J.-H., Jeon, B.-J., Lee, S.-I., Lee, S.-M., Choi, W.-J., 2012. Nitrogen isotope ratios of dissolved organic nitrogen in wet precipitation in a metropolis surrounded by agricultural areas in southern Korea. Agric. Ecosyst. Environ. 159, 161–169.
Leong, J.Y.C., Chong, M.N., Poh, P.E., Hermawan, A., Talei, A., 2017. Longitudinal assessment of rainwater quality under tropical climatic conditions in enabling effective rainwater harvesting and reuse schemes. J. Clean. Prod. 143, 64–75.
Li, C., Li, S.-L., Yue, F.-J., He, S.-N., Shi, Z.-B., Di, C.-L., Liu, C.-Q., 2020. Nitrate sources and formation of rainwater constrained by nitrate isotopes in Southeast Asia: example from Singapore. Chemosphere 241, 125024.
Li, J., Li, R., Cui, L., Meng, Y., Fu, H., 2019. Spatial and temporal variation of inorganic ions in rainwater in Sichuan province from 2011 to 2016. Environ. Pollut. 254, 112941.
Li, S.-L., Calmels, D., Han, G., Gaillardet, J., Liu, C.-Q., 2008. Sulfuric acid as an agent of carbonate weathering constrained by $\delta^{13}C_{DIC}$: examples from Southwest China. Earth Planet Sci. Lett. 270, 189–199.
Li, S.-L., Liu, C.-Q., Li, J., Lang, Y.-C., Ding, H., Li, L., 2010. Geochemistry of dissolved inorganic carbon and carbonate weathering in a small typical karstic catchment of Southwest China: isotopic and chemical constraints. Chem. Geol. 277, 301–309.
Liu, J., Han, G., 2020. Major ions and $\delta^{34}S_{SO4}$ in Jiulongjiang River water: investigating the relationships between natural chemical weathering and human perturbations. Sci. Total Environ. 138208.
Liu, M., Han, G., Zhang, Q., 2020. Effects of agricultural abandonment on soil aggregation, soil organic carbon storage and stabilization: results from observation in a small karst catchment, Southwest China. Agric. Ecosyst. Environ. 288, 106719.
Mullaugh, K.M., Byrd, J.N., Avery, G.B., Mead, R.N., Willey, J.D., Kieber, R.J., 2014. Characterization of carbohydrates in rainwater from the Southeastern North Carolina. Chemosphere 107, 51–57.
Mullaugh, K.M., Hamilton, J.M., Avery, G.B., Felix, J.D., Mead, R.N., Willey, J.D., Kieber, R.J., 2015. Temporal and spatial variability of trace volatile organic compounds in rainwater. Chemosphere 134, 203–209.
Pan, Y.P., Wang, Y.S., Tang, G.Q., Wu, D., 2013. Spatial distribution and temporal variations of atmospheric sulfur deposition in Northern China: insights into the potential acidification risks. Atmos. Chem. Phys. 13, 1675–1688.
Qiao, X., Du, J., Kota, S.H., Ying, Q., Xiao, W., Tang, Y., 2018. Wet deposition of sulfur and nitrogen in Jiuzhaigou National Nature Reserve, Sichuan, China during 2015-2016: possible effects from regional emission reduction and local tourist activities. Environ. Pollut. 233, 267–277.
Qin, C., Li, S.-L., Waldron, S., Yue, F.-J., Wang, Z.-J., Zhong, J., Ding, H., Liu, C.-Q., 2020. High-frequency monitoring reveals how hydrochemistry and dissolved carbon respond to rainstorms at a karstic critical zone, Southwestern China. Sci. Total Environ. 136833.
Rao, P.S.P., Tiwari, S., Matwale, J.L., Pervez, S., Tunved, P., Safai, P.D., Srivastava, A.K., Bisht, D.S., Singh, S., Hopke, P.K., 2016. Sources of chemical species in rainwater during monsoon and non-monsoonal periods over two mega cities in India and dominant source region of secondary aerosols. Atmos. Environ. 146, 90–99.
Rao, W., Han, G., Tan, H., Jin, K., Wang, S., Chen, T., 2017. Chemical and Sr isotopic characteristics of rainwater on the Alxa Desert Plateau, North China: implication for air quality and ion sources. Atmos. Res. 193, 163–172.
Raymond, P.A., Hartmann, J., Lauerwald, R., Sobek, S., McDonald, C., Hoover, M., Butman, D., Striegl, R., Mayorga, E., Humborg, C., Kortelainen, P., Dürr, H., Meybeck, M., Ciais, P., Guth, P., 2013. Global carbon dioxide emissions from inland waters. Nature 503, 355–359.
Silva, M.P.R., Gonçalves, F.L.T., Freitas, S.R., 2009. Two case studies of sulfate scavenging processes in the Amazon region (Rondônia). Environ. Pollut. 157, 637–645.
Singh, A., Agrawal, M., 2008. Acid rain and its ecological consequences. J. Environ. Biol. 29, 15–24.
Song, X., Peng, C., Zhou, G., Jiang, H., Wang, W., 2014. Chinese Grain for Green Program led to highly increased soil organic carbon levels: a meta-analysis. Sci. Rep. 4, 4460.
Szép, R., Bodor, Z., Miklóssy, I., Niță, I.-A., Oprea, O.A., Keresztesi, Á., 2019. Influence of peat fires on the rainwater chemistry in intra-mountain basins with specific atmospheric circulations (Eastern Carpathians, Romania). Sci. Total Environ. 647, 275–289.
Szép, R., Mateescu, E., Niță, I.-A., Birsan, M.-V., Bodor, Z., Keresztesi, Á., 2018. Effects of the Eastern Carpathians on atmospheric circulations and precipitation chemistry from 2006 to 2016 at four monitoring stations (Eastern Carpathians, Romania). Atmos. Res. 214, 311–328.
Tong, X.W., Brandt, M., Yue, Y.M., Ciais, P., Jepsen, M.R., Penuelas, J., Wigneron, J.P., Xiao, X.M., Song, X.P., Horion, S., Rasmussen, K., Saatchi, S., Fan, L., Wang, K.L., Zhang, B., Chen, Z.C., Wang, Y.H., Li, X.J., Fensholt, R., 2020. Forest management in southern China generates short term extensive carbon sequestration. Nature Commun. 11.
Vet, R., Artz, R.S., Carou, S., Shaw, M., Ro, C.-U., Aas, W., Baker, A., Bowersox, V.C., Dentener, F., Galy-Lacaux, C., Hou, A., Pienaar, J.J., Gillett, R., Forti, M.C., Gromov, S., Hara, H., Khodzher, T., Mahowald, N.M., Nickovic, S., Rao, P.S.P., Reid, N.W., 2014. A global assessment of precipitation chemistry and deposition of sulfur, nitrogen, sea salt, base cations, organic acids, acidity and pH, and phosphorus. Atmos. Environ. 93, 3–100.
Walters, W.W., Tharp, B.D., Fang, H., Kozak, B.J., Michalski, G., 2015. Nitrogen isotope composition of thermally produced NOx from various fossil-fuel combustion sources. Environ. Sci. Technol. 49, 11363–11371.
Wang, W.-F., Li, S.-L., Zhong, J., Maberly, S.C., Li, C., Wang, F.-S., Xiao, H.-Y., Liu, C.-Q., 2019. Climatic and anthropogenic regulation of carbon transport and transformation in a karst river-reservoir system. Sci. Total Environ. 135628.
Wang, Z.-J., Li, S.-L., Yue, F.-J., Qin, C.-Q., Buckerfield, S., Zeng, J., 2020. Rainfall driven nitrate transport in agricultural karst surface river system: insight from high resolution hydrochemistry and nitrate isotopes. Agric. Ecosyst. Environ. 291, 106787.
Wang, Z.J., Yue, F.J., Zeng, J., Li, S.L., 2017. The influence of urbanization on karst rivers based on nutrient concentration and nitrate dual isotopes: an example from southwestern China. Acta Geochimica 1–6.
Wei, J., Huang, W., Li, Z., Xue, W., Peng, Y., Sun, L., Cribb, M., 2019a. Estimating 1-km-resolution PM2.5 concentrations across China using the space-time random forest approach. Remote Sens. Environ. 231, 111221.
Wei, J., Li, Z., Cribb, M., Huang, W., Xue, W., Sun, L., Guo, J., Peng, Y., Li, J., Lyapustin, A., Liu, L., Wu, H., Song, Y., 2020. Improved 1 km resolution PM2.5 estimates across China using enhanced space–time extremely randomized trees. Atmos. Chem. Phys. 20, 3273–3289.
Wei, J., Li, Z., Guo, J., Sun, L., Huang, W., Xue, W., Fan, T., Cribb, M., 2019b. Satellite-derived 1-km-resolution PM1 concentrations from 2014 to 2018 across China. Environ. Sci. Technol. 53, 13265–13274.
Wu, Q., Han, G., 2015. Sulfur isotope and chemical composition of the rainwater at the Three Gorges Reservoir. Atmos. Res. 155, 130–140.
Wu, Q., Han, G., Tao, F., Tang, Y., 2012. Chemical composition of rainwater in a karstic agricultural area, Southwest China: the impact of urbanization. Atmos. Res. 111, 71–78.
Wu, L., Wang, S., Bai, X., Tian, Y., Luo, G., Wang, J., Li, Q., Chen, F., Deng, Y., Yang, Y., Hu, Z., 2020. Climate change weakens the positive effect of human activities on karst vegetation productivity restoration in southern China. Ecol. Indicat. 115, 106392.
Xiao, H.Y., Liu, C.Q., 2002. Sources of nitrogen and sulfur in wet deposition at Guiyang, southwest China. Atmos. Environ. 36, 5121–5130.
Xiao, H.Y., Liu, C.Q., 2004. Chemical characteristics of water-soluble components in TSP over Guiyang, SW China, 2003. Atmos. Environ. 38, 6297–6306.
Xu, Z., Wu, Y., Liu, W.-J., Liang, C.-S., Ji, J., Zhao, T., Zhang, X., 2015. Chemical composition of rainwater and the acid neutralizing effect at Beijing and Chizhou city, China. Atmos. Res. 164–165, 278–285.
Yang, F., Tan, J., Shi, Z.B., Cai, Y., He, K., Ma, Y., Duan, F., Okuda, T., Tanaka, S., Chen, G., 2012. Five-year record of atmospheric precipitation chemistry in urban Beijing, China. Atmos. Chem. Phys. 12, 2025–2035.
Yu, G., Jia, Y., He, N., Zhu, J., Chen, Z., Wang, Q., Piao, S., Liu, X., He, H., Guo, X., Wen, Z., Li, P., Ding, G., Goulding, K., 2019. Stabilization of atmospheric nitrogen deposition in China over the past decade. Nat. Geosci. 12 (6), 1–6.
Yue, F.-J., Waldron, S., Li, S.-L., Wang, Z.-J., Zeng, J., Xu, S., Zhang, Z.-C., Oliver, D.M., 2019. Land use interacts with changes in catchment hydrology to generate chronic nitrate pollution in karst waters and strong seasonality in excess nitrate export. Sci. Total Environ. 696, 134062.
Yue, F.J., Li, S.L., Liu, C.Q., Lang, Y.C., Ding, H., 2015. Sources and transport of nitrate constrained by the isotopic technique in a karst catchment: an example from Southwest China. Hydrol. Process. 29, 1883–1893.
Zeng, J., Han, G., 2020. Preliminary copper isotope study on particulate matter in Zhujiang River, southwest China: application for source identification. Ecotoxicol. Environ. Saf. 198, 110663.
Zeng, J., Han, G., Wu, Q., Tang, Y., 2020a. Effects of agricultural alkaline substances on reducing the rainwater acidification: insight from chemical compositions and calcium isotopes in a karst forests area. Agric. Ecosyst. Environ. 290, 106782.
Zeng, J., Han, G., Zhu, J.-M., 2019a. Seasonal and spatial variation of Mo isotope compositions in headwater stream of Xijiang River draining the carbonate terrain, Southwest China. Water 11, 1076.
Zeng, J., Yue, F.-J., Li, S.-L., Wang, Z.-J., Qin, C.-Q., Wu, Q.-X., Xu, S., 2020b. Agriculture

driven nitrogen wet deposition in a karst catchment in southwest China. Agric. Ecosyst. Environ. 294, 106883.
Zeng, J., Yue, F.-J., Wang, Z.-J., Wu, Q., Qin, C.-Q., Li, S.-L., 2019b. Quantifying depression trapping effect on rainwater chemical composition during the rainy season in karst agricultural area, southwestern China. Atmos. Environ. 218, 116998.
Zhang, Y., Han, X., He, N., Long, M., Huang, J., Zhang, G., Wang, Q., Han, X., 2014. Increase in ammonia volatilization from soil in response to N deposition in Inner Mongolia grasslands. Atmos. Environ. 84, 156–162.
Zhang, Z., Chen, X., Cheng, Q., Li, S., Yue, F., Peng, T., Waldron, S., Oliver, D., Soulsby, C., 2020. Coupled hydrological and biogeochemical modelling of nitrogen transport in the karst critical zone. Sci. Total Environ. 138902.
Zhou, X., Xu, Z., Liu, W., Wu, Y., Zhao, T., Jiang, H., Zhang, X., Zhang, J., Zhou, L., Wang, Y., 2019. Chemical composition of precipitation in Shenzhen, a coastal mega-city in South China: influence of urbanization and anthropogenic activities on acidity and ionic composition. Sci. Total Environ. 662, 218–226.